Title	A physical corrosion model for bioabsorbable metal stents
Author(s)	Grogan, James A.; Leen, Sean B.; McHugh, Peter E.
Publication Date	2014
Publication Information	Grogan, JA,Leen, SB,McHugh, PE (2014) 'A physical corrosion model for bioabsorbable metal stents'. Acta Biomaterialia, 10 :2313-2322.
Link to publisher's version	http://dx.doi.org/10.1016/j.actbio.2013.12.059
Item record	http://hdl.handle.net/10379/5408
DOI	http://dx.doi.org/10.1016/j.actbio.2013.12.059

A physical corrosion model for bioabsorbable metal stents

J. A. Grogan, S. B. Leen, P. E. McHugh

Biomechanics Research Centre (BMEC), Mechanical and Biomedical Engineering, National University of Ireland, Galway.

Email: jgrogan.nuig@gmail.com (J. A. Grogan)

Abstract

Absorbable metal stents (AMSs) are an emerging technology in the treatment of heart disease. Computational modelling of AMS performance will facilitate the development of this technology. In this study a physical corrosion model is developed for AMSs based on the finite element method and adaptive meshing. The model addresses a gap between currently available phenomenological corrosion models for AMSs and physical corrosion models which have been developed for more simple geometries than those of a stent. The model developed in this study captures the changing surface of a corroding 3-D AMS structure for the case of diffusion controlled corrosion. Comparisons are made between model predictions and those of previously developed phenomenological corrosion models for AMSs in terms of predicted device geometry and mechanical performance during corrosion. Relationships between alloy solubility and diffusivity in the corrosion environment and device performance during corrosion are also investigated.

Keywords: Finite element analysis; Magnesium; Bioabsorbable stent; Corrosion

1. Introduction

Coronary stents are small tubular scaffolds that are used in the treatment of coronary heart disease. Coronary stents consisting of bioabsorbable metals are an emerging technology which has the potential to address limitations in the current generation of permanent stents, such as in-stent restenosis and late-stent thrombosis [1-3]. These devices have shown promise in early clinical trials [4, 5], however improvements in device performance are still required prior to their adoption in preference to the current generation of permanent stents.

Computational modelling represents a useful method to improve the currently limited understanding of AMS performance in the body and can also be used as part of the device design process [6-9]. In the development of AMSs it is important that the modelling techniques used can account for device corrosion. Previously developed corrosion models for AMS analysis and design have treated the corrosion process in a phenomenological manner. For example, in Grogan et al. [6, 8] uniform corrosion is modelled by specifying a corrosion rate at which the corrosion surface retreats. In order to better understand the corrosion behaviour of AMSs in the body it is important that physical corrosion modelling approaches are also developed for AMSs.

Numerous physical corrosion modelling approaches for metallic alloys have been developed. Many of these rely on the use of boundary element methods and do not consider moving corrosion surfaces [10-13]. Recently, a number of studies have used finite element analysis and adaptive meshing to physically model corrosion [14-16]. In these studies the rate of retreat of the corrosion surface depends on species fluxes at the surface. A study of relevance for AMSs is that of Deshpande [17], who considered the corrosion of a magnesium alloy couple using a physical model with adaptive meshing. The aforementioned physical models have typically been applied to relatively simple geometries: 2-D planar regions, bimetallic interfaces or single corrosion pits. When analysing the corrosion behaviour of an AMS, however, the model must be applied to the complex 3-D structure of the stent. It is the goal of this study to: i) develop a finite element based physical corrosion model that is capable of modelling the corrosion of the complex 3-D structure of a stent using adaptive meshing and ii) apply the model in assessing the performance of a corroding AMS. The development of such a model addresses a gap between currently available phenomenological corrosion models for AMSs and physical corrosion models for more simple geometric configurations.

2. Methods

A thin (20 – 50 nm) oxide film forms on the surface of magnesium and its alloys in atmospheric air [18]. On placement in an aqueous environment the corrosion of magnesium proceeds at local anodes and cathodes on the corrosion surface. For pure magnesium the cathodic regions are often near impurities or rupture locations in the oxide film. Magnesium ions are liberated at the anode and hydrogen gas is evolved at the cathode. The overall electrochemical reaction is:

$$Mg + 2H_20 \rightarrow Mg(OH)_2 + H_2 \quad (1)$$

The resulting $Mg(OH)_2$ is often deposited back onto the corrosion surface, forming a partly protective corrosion layer. The composition and integrity of the corrosion layer depends strongly on the corrosion environment. In environments rich in phosphates and carbonates, such as simulated body fluid (SBF), these ions may be transported into the layer, providing extra structural support [19]. In environments rich in chlorine ions the $Mg(OH)_2$ may be converted into highly soluble $MgCl_2$, reducing the integrity of the layer [20]. If the layer is not sufficiently protective in certain regions corrosion can proceed in these regions at a relatively high rate. This can lead to localized corrosion and undermining of the corrosion layer. Overall, the corrosion behaviour of magnesium is therefore largely governed by the integrity of the partly protective corrosion layer. If the layer is deposited more quickly than it is broken down a reduced corrosion rate results, as reactants must be transported through it [21-23].

Corrosion can be modelled by considering two primary processes, the electrochemical reaction at the corrosion surface and the transport of ions to and from the corrosion surface. If ions are transported to or from the corrosion surface more quickly than the rate of their production in the electrochemical reaction the corrosion process is deemed to be primarily activation controlled [24]. Conversely, if the transport of ions is slower than the rate of reaction the process is primarily transport controlled. In the latter case this can result in the concentration of metallic ions at the corrosion surface reaching the saturation concentration of the solution. This study is predicated on a transport controlled process, based on the assumption that metallic ion transport, particularly diffusion, is slower than the electrochemical reaction rate for implants surrounded by layers of corrosion product and tissue in the body.

The focus of this paper is the corrosion of pure magnesium, without impurities. Modelling of micro-galvanic corrosion in the vicinity of impurities or secondary phases in alloys introduces significant extra complexity, as the corrosion surface evolves in a complicated manner at the boundary with the matrix and cannot be easily captured using a 3-D adaptive meshing approach. An alternate approach is suggested for modelling micro-galvanic corrosion with secondary phases and impurities in the Limitations section.

The physical corrosion model used in this study is first described. It is assumed that the corrosion of the AMS is governed by the diffusion of metallic ions from the corrosion surface, with the rate of retreat of the corrosion surface being related to the flux of metallic ions into solution. The implementation of the model in the commercial implicit finite element (FE) code Abaqus/Standard is then described, based on the use of user-defined subroutines. It is verified that the predictions of the FE implementation of the corrosion model are in agreement with the analytical solution of a 1-D moving boundary diffusion problem. Finally, the model is applied in analysing the corrosion of an AMS.

The transport of a species i in solution can be generally described through the Nernst-Plank equation [14]:

$$\boldsymbol{N}_i = -D_i \boldsymbol{\nabla} c_i + \boldsymbol{V} c_i - \frac{z_i D_i F c_i}{RT} \boldsymbol{\nabla} \phi \tag{2}$$

where $\boldsymbol{\nabla} a$ is the gradient vector of the scalar field a, $\boldsymbol{N}_i$ is the species flux vector, D_i is the diffusion coefficient, c_i is the species concentration, $\boldsymbol{V}$ is the solution velocity vector, ϕ is the potential, z_i is the charge and F, R and T are Faraday's constant, the universal gas constant and temperature respectively. This equation represents the flux of a species under diffusion, migration in a potential field and convection.

The conservation of flux for species i is then:

$$\frac{\partial c_i}{\partial t} = -\boldsymbol{\nabla} \cdot \boldsymbol{N}_i \tag{3}$$

From Eqns. 2 and 3 it can be seen that the movement of ions through a solution is governed by the concentration gradient, the potential gradient and the fluid velocity. For the purposes of this study it is assumed that diffusion is the rate limiting process in the transport of reactants, i.e. that fluid velocity and potential gradient have negligible influence. Such an assumption may be appropriate for AMSs in cases where there is a physical barrier to the migration and convection of species surrounding the device, through which reactants must diffuse. Practically, this barrier may take the form of a polymer coating, a layer of deposited corrosion product or surrounding tissue (in cases where convective transport in the tissue is negligible). In these cases Eqns. 2 and 3 reduce to Fick's law:

$$\frac{\partial c_i}{\partial t} = -\boldsymbol{\nabla} \cdot (D_i \boldsymbol{\nabla} c_i) \tag{4}$$

A further assumption in this study is that the transport and solubility of metallic ions in solution govern the underlying rate of chemical reactions associated with the corrosion process. Given that magnesium alloy stents are the most promising candidates for AMSs to date [4, 5], the diffusion of Mg ions is the focus of this study, such that Eqn. 4 becomes:

$$\frac{\partial c_{Mg}}{\partial t} = -\boldsymbol{\nabla} \cdot \left(D_{Mg} \boldsymbol{\nabla} c_{Mg}\right) \tag{5}$$

where the subscript 'Mg' pertains to magnesium ions and is henceforth omitted. As magnesium dissolves in solution, the corrosion surface moves, leading to a moving boundary problem. As the corrosion surfaces moves, mass must be conserved in the solid and solution.

Based on the assumption of transport rather than activation controlled corrosion, this leads to the following Rankine-Hugoniot condition on the moving corrosion surface (see Scheiner and Hellmich [24]):

$$\{-D\boldsymbol{\nabla} c - (c_{sol} - c_{sat})\boldsymbol{v}\} \cdot \boldsymbol{n} = 0 \tag{6}$$

where c_{sol} is the concentration of magnesium ions in the solid, c_{sat} is the saturation concentration of magnesium ions in solution, $\boldsymbol{v}$ is the corrosion surface velocity vector and $\boldsymbol{n}$ is the corrosion surface normal vector. Eqns. 5 and 6 amount to a Stefan problem, for which analytical solutions have been derived for simple geometries [25]. A schematic of the final assumed corrosion process is shown in Fig. 1.

To implement Eqns. 5 and 6 in Abaqus the arbitrary Lagrangian-Eulerian (ALE) adaptive meshing functionality is used. This functionality allows moving boundary problems to be solved by including an Eulerian stage in each analysis increment in which nodes in the FE mesh can be moved independently of the underlying material. To implement the corrosion model on the complex 3-D structure of the stent a facet based approach, previously developed in Grogan et al. [8], is adopted. In this approach, the corrosion surface is divided into facets (triangles formed by three adjacent nodes in the FE mesh). During corrosion each facet can move inwards along its inward pointing normal vector, $\boldsymbol{n}$ at a prescribed velocity v. Nodes on the FE mesh follow the motion of their underlying facets during the Eulerian stage of the analysis increment.

To implement the physical corrosion model it is necessary to prescribe a suitable velocity v for each facet along its inward pointing normal vector, $\boldsymbol{n}$, on the corrosion surface. Based on Eqn. 6 this can be given as:

$$v = \frac{D(\nabla c \cdot \boldsymbol{n})}{c_{sol} - c_{sat}} \tag{7}$$

The identification of the quantity $\nabla c \cdot \boldsymbol{n}$ is not trivial in this case. The approach taken here is shown in Fig. 2. The facet outward pointing normal is projected into the element containing the facet on the solution side of the interface. The concentration at the point of intersection of the outward normal and the element faces, c_i, is then found. The quantity $\nabla c \cdot \boldsymbol{n}$ is then given by $c_i - c_{sat}$.

A flowchart for the implementation of the model in an Abaqus UMESHMOTION user subroutine is given in Fig. 3. To test the implementation of the newly developed model, predictions are compared to a 1-D analytical model based on similarity solutions to Stefan problems used by Javierre et al. [26] for solidification problems and adopted here for the case of diffusion controlled corrosion. As shown in Fig. 4, the corrosion domain is split into two parts, solid and liquid. The initial length of the solid domain is 0.2 mm and the length of the liquid domain is 4.8 mm. The initial concentration of magnesium in solution, c_0, is 0.0 kg/m^3. c_{sol} is 1735 kg/m^3, which is the mass density of pure magnesium. c_{sat} is 134.0 kg/m^3, which is the solubility of magnesium chloride in water at 25 °C [27]. The saturation concentration of magnesium ions in solution depends strongly on the temperature, pH and the availability of other ions, such as chlorine. For example, in the absence of chlorine ions, magnesium hydroxide is formed, which has a low solubility in water and leads to a c_{sat} value of 0.0048 kg/m^3 [27]. The diffusivity, D, of magnesium ions in biological fluids has not been widely reported. As a result, a value of 0.10575 mm^2/hr is assumed here, based on the diffusivity of magnesium in sea water [28]. Given that the saturation concentration and diffusivity used here are not based on in-vivo measurements, owing to a lack of published data, a more detailed investigation for a range of saturation concentrations and diffusivities is reported later in this study when investigating full stent geometries. It should be further noted that these diffusivity and saturation values are based on room temperature measurements or measurements at 25 °C, while in the body corrosion occurs at a temperature of approximately 37 °C. This higher temperature would typically imply an increase in the assumed diffusivity and saturation concentration values.

The movement of the corrosion interface over time is given by [25]:

$$s(t) = s_0 + 2\alpha\sqrt{t} \tag{8}$$

where $s(t)$ and s_0 are the current and initial interface positions respectively and α is obtained through solving:

$$\alpha = \frac{c_0 - c_{sat}}{c_{sol} - c_{sat}} \sqrt{\frac{D}{\pi}} \frac{exp\left(\frac{-\alpha^2}{D}\right)}{erfc\left(\frac{-\alpha}{\sqrt{D}}\right)} \tag{9}$$

The concentration of magnesium in the solid and solution at position x is then:

$$c(x,t) = \begin{cases} c_{sol} & if\ x < s(t) \\ c_0 + \dfrac{(c_{sat} - c_0)erfc\left((x - s_0)/(2\sqrt{Dt})\right)}{erfc\left(\frac{\alpha}{\sqrt{D}}\right)} & if\ x \geq s(t) \end{cases} \tag{10}$$

The corrosion of a stent repeating unit in solution is modelled using the ALE model and the Abaqus/Standard solver. The geometries of the stent and corrosion environment are shown in Fig. 5. Both the stent and surrounding environment are meshed using 3-D linear coupled temperature-displacement reduced integration brick elements (C3D8RT). This element is chosen as it facilitates the use of both adaptive meshing and the solution of the diffusion problem, through the analogous nature of the governing equations for diffusion and heat transfer [29].

The design of the stent is generic and based on those used in the previous studies of Grogan et al [7, 8]. However, due to the use of a repeating sinusoidal ring pattern it is representative of many currently available commercial stents, in particular the CYPHER and Biotronik DREAMS platforms. The initial stent strut thickness and width are both 120 μm, which are representative of the dimensions of the Biotronik DREAMS magnesium stent [30]. The stent geometry is obtained through the simulated expansion of a stent unit with a stiff inner cylinder (see Grogan et al. [7] for details).

The residual stress-state in the device is not considered during corrosion. This is based on the finding by Grogan et al. [8] that for a given stent design, the same fraction of stiffness or strength is lost for a given amount of mass lost under uniform corrosion, regardless of the initial stiffness or strength. The residual stress state itself is also assumed not to influence the corrosion process in this study. This assumption is further discussed subsequently. The stent elastic-plastic mechanical properties are assumed to be those of the AZ31 magnesium alloy, given in Grogan et al. [8].

The coefficients used for the 1-D analytical model are adopted for the stent model. Since the saturation concentration and diffusivity of magnesium in human blood are not widely reported, the sensitivity of stent corrosion behaviour to changes in these values is investigated. The differences in corroded device geometry and mechanical integrity predictions for the physical model and the phenomenological model developed in Grogan et al. [8] are also investigated, by simulating the corrosion of the stent assuming a constant corrosion rate on all facets (i.e. v in Eqn. 7 is assumed constant). While the phenomenological model of Grogan et al. [8] also considered (randomly-distributed) pitting corrosion in AZ31 alloy, this behaviour is not consistent with the diffusion controlled corrosion of the homogeneous pure magnesium considered in this study. For this reason, only the uniform corrosion aspect of the phenomenological model is considered.

The corrosion model developed in this study has attractive computational efficiency. AMS corrosion simulations are performed on a single quad-core Intel i7 processor on a Dell XPS PC, each requiring approximately four CPU hours.

3. Results

Fig. 6 shows a comparison of (a) corrosion surface displacement and (b) magnesium ion concentration predicted by the ALE corrosion model and given by the 1-D analytical model. There is good agreement between the models, verifying the applicability of the ALE adaptive meshing algorithm in Abaqus for Stefan problems of this type.

Fig. 7 (a) shows a contour plot of predicted magnesium ion concentration in the corrosive environment over time. As the device corrodes its dimensions are reduced. The initially sharp edges of the device are rounded as corrosion progresses, as shown in Fig. 7 (b). This is expected for the diffusion controlled corrosion of geometries with sharp edges [31].

To test model sensitivity to magnesium saturation concentration and diffusivity parameters, simulations are performed for a range of saturation concentrations (between 13.4 kg/m^3 and 134.0 kg/m^3) and for a range of diffusivities (between 0.010575 mm^2/hr and 0.50575 mm^2/hr). From the overall generated dataset, mass loss versus time profiles are shown in Fig. 8 for two different magnesium saturation concentrations and four different diffusivities. In this case mass loss M is expressed as the loss in stent mass divided by original mass.

It is observed that the mass loss is largely proportional to the square root of time in solution. This relationship can be characterised by a constant of proportionality A such that for a given diffusivity:

$$M = A\sqrt{t} \tag{11}$$

The values of A are indicated in Figs. 8 (a) and 8 (b) for the relevant examples. Values of A for the full set of simulations are plotted in Fig. 9 (a). From this it can be observed that, for a given diffusivity, A is itself proportional to the saturation concentration, giving:

$$A = Bc_{sat} \tag{12}$$

As shown in Fig. 9 (b), the slope of this proportional relationship B increases with increasing diffusivity according to a power law, giving the following fit:

$$B = 0.0334D^{0.57} \tag{13}$$

Using these findings and substituting Eqns. 12 and 13 into Eqn. 11, it is possible to approximate the mass loss for the stent analysed here over a range of diffusivities and saturation concentrations through the following relationship:

$$M = 0.0334D^{0.57}c_{sat}\sqrt{t} \tag{14}$$

or in rate form:

$$\frac{dM}{dt} = \frac{\alpha D^{\beta} c_{sat}}{\sqrt{t}} \tag{15}$$

where α and β are constants, equal to 0.017 and 0.57 respectively. Based on Eqn. 15 it is predicted that doubling the diffusivity of the alloy in the corrosion environment increases the mass loss rate by a factor of approximately 1.48.

Fig. 10 (a) shows predicted mass loss versus time for the phenomenological and physical FE corrosion models and the prediction of Eqn. 14. There is good agreement between Eqn. 14 and the physical FE model. It is noted that the mass loss rate is largely constant for the phenomenological model due to the assumption of a constant input corrosion rate. Although not performed here, it is noted that it is possible to modify the input corrosion rate over time for the phenomenological model such that both the phenomenological and physical corrosion models have identical mass loss rates. Fig. 10 (b) shows a comparison of the geometries of the AMS following corrosion with the physical and phenomenological models for the same amount of mass loss. While the geometries are largely similar, the physical corrosion model expectedly predicts more rounded edges and also less corrosion in the inside of hinges, where there are lower concentration gradients and more corrosion on the outside of hinges.

Figs. 11 (a) and (b) show predicted losses in radial stiffness (change in resistive force for an applied reduction in stent diameter) and radial strength (force required to crimp the stent back to its unexpanded diameter) with corrosion for the physical and phenomenological models. There is close agreement between the predictions of both models, suggesting that the phenomenological model of Grogan et al. [8] may be suitable for predicting the mechanical performance of AMSs undergoing diffusion controlled corrosion.

4. Discussion

A physical corrosion model is developed here for complex 3-D geometries, based on the use of ALE adaptive meshing. The model, implemented in the Abaqus commercial finite element solver shows good agreement with the analytical solution of a 1-D moving boundary diffusion corrosion problem and represents a first attempt at modelling the corrosion of AMSs using a physical, rather than phenomenological, approach. The verification performed here is also the first verification, to the authors' knowledge, of the applicability of the ALE adaptive meshing algorithm in Abaqus for the solution of Stefan type problems.

The rounding of the initially sharp edges in the strut is expected for a diffusion controlled corrosion process [31]. The dependence of stent mass loss on the square root of time, manifested in Eqn. 14, is analogous to, and indeed is likely to follow from, the relationship between corrosion surface position and time for the 1-D corrosion problem, given in Eqn. 8 and shown in Fig. 6 (a). It is interesting that such a relationship still holds here, despite the complex geometry of the stent.

Eqn. 15 gives a number of useful insights into the corrosion of AMSs. It predicts that the mass loss rate is proportional to the saturation concentration of magnesium ions in solution. This facilitates predictions of corrosion rates in variety of environments, which is of particular importance given that the solubility of magnesium ions depends strongly on the availability of chlorine ions in solution [20]. The dependence of mass loss rate on diffusivity is also of interest, given that a range of effective diffusivity values may be applicable depending on whether the device is embedded in polymer, tissue or corrosion product.

It is noted that the predicted corrosion time for the stent in Fig. 8 is on the order of 30 minutes. This is significantly less than the time of one to three months that would be expected in a clinical setting. This is attributed here to the use of the saturation concentration of magnesium chloride (134 kg/m^3) as a basis for the study. Magnesium chloride is regarded to highly soluble in aqueous environments, and its formation is associated with the high corrosion rates of magnesium in the presence of chloride ions [20]. Magnesium hydroxide, which forms in the absence of chloride ions, has a far lower solubility however (0.0048 kg/m^3). Due to the presence of chloride ions in the blood a saturation concentration between the extreme values of 134 kg/m^3 and 0.0048 kg/m^3 would be expected. Using Eqn. 14 and assuming a mass loss of 30 % and diffusivity of 0.10575 mm^2/hr, the saturation concentration to give a corrosion time of three months is 0.69 kg/m^3. This concentration falls reasonably between the extreme values for magnesium chloride and hydroxide formation.

The physical and phenomenological corrosion models are in good agreement regarding predictions of device mechanical integrity for the same amount of mass lost, although as shown in Fig. 10 (a), the predicted amount of mass lost over time is different for both models. This difference can potentially be addressed through modifying the input corrosion rate for the phenomenological model, such that output mass loss rates are in agreement for both models. Based on this approach, this suggests that the phenomenological model developed in Grogan et al. [8] is suitable for modelling the effects of at least diffusion controlled corrosion, where suitable input corrosion rates for the phenomenological corrosion model can be identified through the use of the physical model and Eqn. 14.

Regarding the overall poor clinical outcomes from the first AMS trial, it is acknowledged that this was due to both inflammation (45 %) and loss of stent mechanical integrity (42 %) [32]. Drug coatings have been used on subsequent devices and have demonstrably reduced inflammation [30]. In terms of device structural integrity, the primary concern is undoubtedly mitigating pitting corrosion. The authors have shown that pitting corrosion leads to order of magnitude reductions in the duration of device integrity [6, 8]. One of the primary methods of reducing pitting corrosion is ensuring minimal impurity (particularly iron) content in the precursor material [33]. For devices undergoing uniform corrosion, increasing strut widths within the tight limits of the ductility of magnesium alloys leads to some improvement in scaffolding duration [8].

Regarding microstructure, smaller grain sizes reduce corrosion rates [34, 35]. It is also suggested that certain microstructures can behave as barriers to the corrosion process due to the geometry of secondary phases [33]. The texture in the microstructure plays an important role in determining overall device mechanics and can be tailored to give ideal mechanical [36] and corrosion performance [37, 38].

5. Limitations

The physical corrosion model developed here gives a number of useful insights into AMS corrosion. However, the assumption of corrosion driven by magnesium diffusion alone limits its applicability.

The assumption of diffusion rather than activation control is based on observations of the formation of stable layers of corrosion product in the body [39 - 41], or tissue layers [42], and the known diffusion controlled corrosion process associated with stable corrosion product layers [21-23]. The assumption that diffusion is governed by the transport of magnesium ions only requires experimental validation. It may be the case that in-vivo diffusion is controlled by hydrogen transport at the cathode or more complex magnesium ion diffusion and chemical reaction processes within the corrosion product layer [21, 39]. One useful test that could be used for the model is to compare predicted mass loss profiles with the results of pencil electrode tests [43]. Previous studies have used this approach to demonstrate the predictive capability of similar 1-D moving boundary diffusion simulations for the corrosion of stainless steel [24]. The predictive capability of the present model could be greatly improved by adding the ability to explicitly model the reaction kinetics between magnesium and hydroxide ions at the corrosion surface and resulting corrosion product deposition, as per [15].

The presented model does not capture the experimentally observed increase in magnesium stent fractures in hinge regions [44, 45]. While the model is developed to allow the corrosion behaviour to have a dependence on the local stress state, the underlying cause of the increased fracture rate in hinges has not been clearly identified. Certainly it is known that certain magnesium alloys are subject to stress corrosion cracking in simulated body fluid [46], however the possibilities of the fractures being due to oxide layer cracking at the hinges during deployment, increased dislocation density in hinge regions or a combination of localized corrosion and increased load bearing on hinges have not been discounted.

The material used in this study is pure magnesium. The corrosion of magnesium containing impurities or secondary phases is initially a micro-galvanic process. Due to large potential differences at the interface between the matrix and secondary phases significant mass loss can occur in these regions. This highly localized mass loss makes tracking the evolution of the specimen geometry challenging if adaptive meshing is used [15]. An alternate approach for this situation is the use of Level Sets and the Extended Finite Element method [47]. This approach is the topic of on-going research by the authors. Once a stable corrosion product layer develops the micro-galvanic corrosion process may become diffusion controlled. Under this condition the predictions of the present model may be valid.

In this study it is assumed that the stent is already covered by a stable corrosion product layer (or polymer coating or tissue layer). The corrosion of the stent up to the time of the formation of the corrosion product layer is not considered, as this behaviour cannot be assumed to be diffusion controlled. A model that can be used in that scenario is that of Sun et al. [15]. Thus, the present methodology is most suited to longer term device corrosion, once a stable corrosion layer has already formed.

6. Conclusions

A physical model is developed that uses the ALE adaptive meshing method to model the diffusion controlled corrosion of a 3-D absorbable metal stent (AMS) geometry. Assuming that the corrosion rate is governed by the diffusion of magnesium ions in solution, it is predicted that the mass loss rate from the AMS is inversely proportional to the square root of immersion time. It is predicted that the mass loss rate is proportional to the saturation concentration of magnesium ions in solution and is related to the diffusivity of magnesium ions in solution through a power law behaviour, where doubling the diffusivity increases the mass loss rate by a factor of approximately 1.48. The physical model developed here is computationally efficient and can serve as a useful accompaniment to existing phenomenological models used in the analysis and design of AMSs.

7. Acknowledgements

The authors acknowledge funding through an Irish Research Council (IRC) scholarship (J. A. Grogan) under the EMBARK initiative.

8. References

[1] Mitra, A.K., Agrawal, D.K., 2006. In stent restenosis: bane of the stent era. J ClinPathol 59, 232 – 239.

[2] Ong, A.T.L., McFadden, E.P., Regar, E., De Jaegere, P.P.T., Van Domburg, R.T., Serruys, P.W., 2005. Late angiographic stent thrombosis (LAST) events with drug-eluting stents. J Am Coll Cardiol 45, 2088–92.

[3] Waksman, R., 2006. Biodegradable stents: they do their job and disappear. J Invasive Cardiol 18, 70–74.

[4] Erbel, R., Di Mario, C., Bartunek, J., Bonnier, J., De Bruyne, B., Eberli, F.R., Erne, P., et al., 2007. Temporary scaffolding of coronary arteries with bioabsorbable magnesium stents: a prospective, non-randomised multicentre trial. Lancet 369, 1869–75.

[5] Haude, M., Erbel, R., Erne, P., Verheye, S., Degen, H., Böse, D., Vermeersch, P., et al., 2013. Safety and performance of the drug-eluting absorbable metal scaffold (DREAMS) in patients with de-novo coronary lesions: 12 month results of the prospective, multicentre, first-in-man BIOSOLVE-I trial. Lancet 6736, 1–9.

[6] Grogan, J.A, O'Brien, B.J., Leen, S., McHugh, PE., 2011. A corrosion model for bioabsorbable metallic stents. Acta Biomater 7, 3523–33.

[7] Grogan, J.A., Leen, S.B., McHugh, P.E., 2012. Comparing coronary stent material performance on a common geometric platform through simulated bench-testing. J Mech Behav Biomed Mater 12, 129-138.

[8] Grogan, J.A., Leen, S.B., McHugh, P. E., 2013. Optimizing the design of a bioabsorbable metal stent using computer simulation methods. Biomaterials 34, 8049-60.

[9] Wu, W., Gastaldi, D., Yang, K., Tan, L., Petrini, L., Migliavacca, F., 2011. Finite element analyses for design evaluation of biodegradable magnesium alloy stents in arterial vessels. Mater Sci Eng B 176, 1733-40.

[10] Jia, J.X., Song, G., Atrens, A., St John, D., Baynham, J., Chandler, G., 2004. Evaluation of the BEASY program using linear and piecewise linear approaches for the boundary conditions. Mater Corros 55, 845–852.

[11] Jia, J. X., Song, G., Atrens, A., 2007. Experimental measurement and computer simulation of galvanic corrosion of magnesium coupled to steel. Adv Eng Mater 9, 65–74.

[12] Jia, J.X., Song, G., Atrens, A., 2006. Influence of geometry on galvanic corrosion of AZ91D coupled to steel. Corros Sci 48, 2133–53.

[13] Shi, Z., Jia, J.X., Atrens, A., 2012. Galvanostatic anodic polarisation curves and galvanic corrosion of high purity Mg in 3.5% NaCl saturated with Mg(OH)2. Corros Sci 60, 296–308.

[14] Deshpande, K.B., 2010. Validated numerical modelling of galvanic corrosion for couples: Magnesium alloy (AE44)–mild steel and AE44–aluminium alloy (AA6063) in brine solution. Corros Sci 52, 3514–22.

[15] Sun, W., Liu, G., Wang, L., Wu, T., 2012. An arbitrary Lagrangian – Eulerian model for studying the influences of corrosion product deposition on bimetallic corrosion. J Solid State Electrochem 17, 829-840.

[16] Xiao, J., Chaudhuri, S., 2011. Predictive modeling of localized corrosion: An application to aluminum alloys. Electrochim Acta 56, 5630–5641.

[17] Deshpande, K.B., 2011. Numerical modeling of micro-galvanic corrosion. Electrochim Acta 56, 1737–45.

[18] Kutz, M., Handbook of Materials Selection, Wiley ,USA, 2002.

[19] Kalb, H., Rzany, A., & Hensel, B., 2012. Impact of microgalvanic corrosion on the degradation morphology of WE43 and pure magnesium under exposure to simulated body fluid. Corros Sci 57, 122–130.

[20] Witte, F., Hort, N., Vogt, C., Cohen, S., Kainer, K.U., Willumeit, R., Feyerabend, F., 2008. Degradable biomaterials based on magnesium corrosion. Curr Opin Solid State Mater Sci 12, 63–72.

[21] Song, Y., Shan, D., Chen, R., Zhang, F., Han, E.H., 2009. Biodegradable behaviors of AZ31 magnesium alloy in simulated body fluid. Mat Sci Eng C 29, 1039–1045.

[22] Bender, S., Goellner, J., Heyn, A., Boese, E., 2007. Corrosion and corrosion testing of magnesium alloys. Mater Corros 58, 977–982.

[23] Feliu, S., Maffiotte, C., Galván, J. C., Barranco, V., 2011. Atmospheric corrosion of magnesium alloys AZ31 and AZ61 under continuous condensation conditions. Corrosion Science, 53, 1865–1872.

[24] Scheiner, S., Hellmich, C., 2007. Stable pitting corrosion of stainless steel as diffusion-controlled dissolution process with a sharp moving electrode boundary. Corros Sci 49, 319–346.

[25] Crank, J., 1987. Free and Moving Boundary Problems (Oxford Science Publications). Oxford University Press, USA.

[26] Javierre, E., Vuik, C., Vermolen, F.J., Van der Zwaag, S., 2006. A comparison of numerical models for one-dimensional Stefan problems. J Comput App Math 192, 445–459.

[27] Hill G., Holman., J.S. Chemistry in Context. Nelson Thornes, 2000.

[28] Yan, J.F., Nguyen, T.V., White, R.E., Griffin, R.B., 1993. Mathematical modeling of the formation of calcareous deposits on cathodically protected steel in seawater. J Electrochem Soc 140, 3.

[29] Hose, D. R., Narracott, A. J., Griffiths, B., Mahmood, S., Gunn, J., Sweeney, D., Lawford, P. V., 2004. A thermal analogy for modelling drug elution from cardiovascular stents. Comp Method Biomech Biomed Eng 7, 257–64.

[30] Haude, M., Erbel, R., Erne, P., Verheye, S., Degen, H., Böse, D., Vermeersch, P, et al., 2013. Safety and performance of the drug-eluting absorbable metal scaffold (DREAMS) in patients with de-novo coronary lesions: 12 month results of the prospective, multicentre, first-in-man BIOSOLVE-I trial. Lancet, 6736, 1–9.

[31] Rathjen, K. A., Jiji, L. M., 1971. Heat conduction with melting or freezing in a corner. J H Tran, 93, 101.

[32] Erbel, R., Di Mario, C., Bartunek, J., Bonnier, J., de Bruyne, B., Eberli, F., Haude, M., et al.., 2007. Temporary scaffolding of coronary arteries with bioabsorbable magnesium stents: a prospective, non-randomised multicentre trial. Lancet, 369, 1869–75.

[33] Song, G., Atrens, A., 2003. Understanding magnesium corrosion—A framework for improved alloy performance. Adv Eng Mater, 5, 837–858.

[34] Alvarez-Lopez, M., Pereda, M. D., del Valle, J. A, Fernandez-Lorenzo, M., Garcia-Alonso, M. C., Ruano, O. A, Escudero, M. L. 2010. Corrosion behaviour of AZ31 magnesium alloy with different grain sizes in simulated biological fluids. Acta Biomater, 6, 1763–71.

[35] Zhou, W., Shen, T., Aung, N. N., 2010. Effect of grain size and twins on corrosion behaviour of AZ31B magnesium alloy. Corros Sci 52, 1035–1041.

[36] Vedani, M., Ge, Q., Wu, W., Petrini, L. (2012). Texture effects on design of Mg biodegradable stents. Int J Mater Forming, 1–8.

[37] Xin, R. L., Wang, M. Y., Gao, J. C., Liu, P., Liu, Q., 2009. Effect of microstructure and texture on corrosion resistance of magnesium alloy. Mater Sci Forum 610-613, 1160–1163.

[38] Song, G. L., 2012. The effect of texture on the corrosion behavior of AZ31 Mg alloy. JOM 64, 671–679.

[39] Bowen, P. K., Drelich, J., Goldman, J., 2013. Magnesium in the murine artery: Probing the products of corrosion. Acta Biomater, In Press.

[40] Wittchow, E., Adden, N., Riedmüller, J., Savard, C., Waksman, R., Braune, M., 2013. Bioresorbable drug-eluting magnesium-alloy scaffold: design and feasibility in a porcine coronary model. EuroIntervention 8, 1441–50.

[41] Witte, F., Fischer, J., Nellesen, J., Vogt, C., Vogt, J., Donath, T., Beckmann, F., 2010. In vivo corrosion and corrosion protection of magnesium alloy LAE442. Acta Biomater 6, 1792–9.

[42] Badar, M., Lünsdorf, H., Evertz, F., Rahim, M. I., Glasmacher, B., Hauser, H., Mueller, P. P., 2013. The formation of an organic coat and the release of corrosion microparticles from metallic magnesium implants. Acta Biomater 9, 7580–9.

[43] Ernst, P., Newman, R., 2002. Pit growth studies in stainless steel foils. I. Introduction and pit growth kinetics. Corrosion Science 44, 927–941.

[44] Deng, C. Z., Radhakrishnan, R., Larsen, S. R., Boismer, D. A., Stinson, J. S., Hotchkiss, A. K., Petersen, E. M., et al., 2011. Magnesium alloys for bioabsorbable stents: a feasibility assessment. In Magnesium Technology 2011. Wiley, USA,

[45] Wu, W., Chen, S., Gastaldi, D., Petrini, L., Mantovani, D., Yang, K., Tan, L., et al., 2013. Experimental data confirm numerical modeling of the degradation process of magnesium alloys stents. Acta Biomater 9, 8730–8739.

[46] Winzer, N., Atrens, A., Song, G., Ghali, E., Dietzel, W., Kainer, K. U., Hort., N., et al., 2005. A critical review of the stress corrosion cracking (SCC) of magnesium alloys. Adv Eng Mater 7, 659–693.

[47] Chessa, J., Smolinski, P., Belytschko, T., 2002. The extended finite element method (XFEM) for solidification problems. Int J Num Method Eng, 53, 1959–1977.

9. Figure Captions

Fig. 1 A sketch of the assumed corrosion process. The concentration of magnesium ions c in the magnesium alloy is assumed to have a constant value, c_{sol}. As the alloy corrodes magnesium ions (Mg^{++}) are dissolved in the corrosion environment. The magnesium ions diffuse through the corrosion environment, which has a maximum solubility for the ions of c_{sat} and diffusivity D. As the magnesium ions dissolve, the movement of the boundary between the alloy and environment (i.e. the corrosion surface) moves into the alloy with velocity vector $\boldsymbol{v}$.

Fig. 2 A finite element model of a magnesium component in a corrosive environment. The concentration gradient at the corrosion surface is approximated by projecting an outward normal, $\boldsymbol{n}$, from the centroid of each facet, 'a'. The concentration in the corrosive environment is evaluated at point 'b', which is the intercept of the normal and the faces of element adjacent to the facet.

Fig. 3 A flowchart for the implementation of the corrosion model using the UMESHMOTION subroutine and the Abaqus/Standard solver.

Fig. 4 A schematic of the 1-D corrosion problem solved analytically and using the physical corrosion model.

Fig. 5 Finite element model of a stent ring embedded in a corrosive environment. Due to the symmetry of the problem one 12th of the geometry is modelled. The corrosion environment is an annulus of length 1.47 mm, inner diameter 0.88 mm and outer diameter is 4.88 mm. The stent length is 1.1 mm, the initial outer diameter is 1.2 mm and the expanded outer diameter is 2.94 mm. The strut width and thickness are both 0.12 mm.

Fig. 6 A comparison of the predictions of the physical corrosion model and the corresponding analytical solution to the Stefan problem. The predicted movement of the corrosion surface over time is shown in (a) and the predicted evolution of the concentration of magnesium ions in the solid and solution during corrosion is shown in (b).

Fig. 7 Contour plots of predicted magnesium ion concentration in kg/m^3 in the corrosive environment over time. In (a) the upper half of the model has been removed for illustrative purposes. Grey regions correspond to non-corroded metal. (b) Illustration of the changing dimensions of a cross-section of the hinge as it corrodes. In this case D = 0.10575 mm^2/hr and c_{sat} = 134.0 kg/m^3.

Fig. 8 Predicted loss in mass with time for a saturation concentration of (a) 134.0 kg/m^3 and (b) 13.4 kg/m^3, each for four different diffusivities. Linear best fits of slope '*A*' hr$^{-0.5}$ are also shown in red for each set of data.

Fig. 9 (a) Predicted change in the constant of proportionality '*A*' from Fig. 8 with increasing saturation concentration. Linear best fits of slope '*B*' m^3/(kg√hr) are also shown for each set of data. (b) Predicted change in the constant of proportionality '*B*' from Fig. 9 (a) with increasing diffusion coefficient. A power-law best fit is included.

Fig. 10 (a) Comparison of mass lost over time predicted by the physical and phenomenological corrosion FE models and Eqn. 14. (b) Comparison of the stent geometry at 70 % mass loss for both models. The physical corrosion model is shown in red and the phenomenological model is overlaid in transparent green. The physical model predicts greater mass loss on the outside of the hinge and less mass loss on the inside of the hinge than the phenomenological model.

Fig. 11 (a) Predicted loss in radial stiffness and strength with mass loss for the physical and phenomenological corrosion models. (b) Predicted loss in radial stiffness and strength with time for the physical corrosion model.

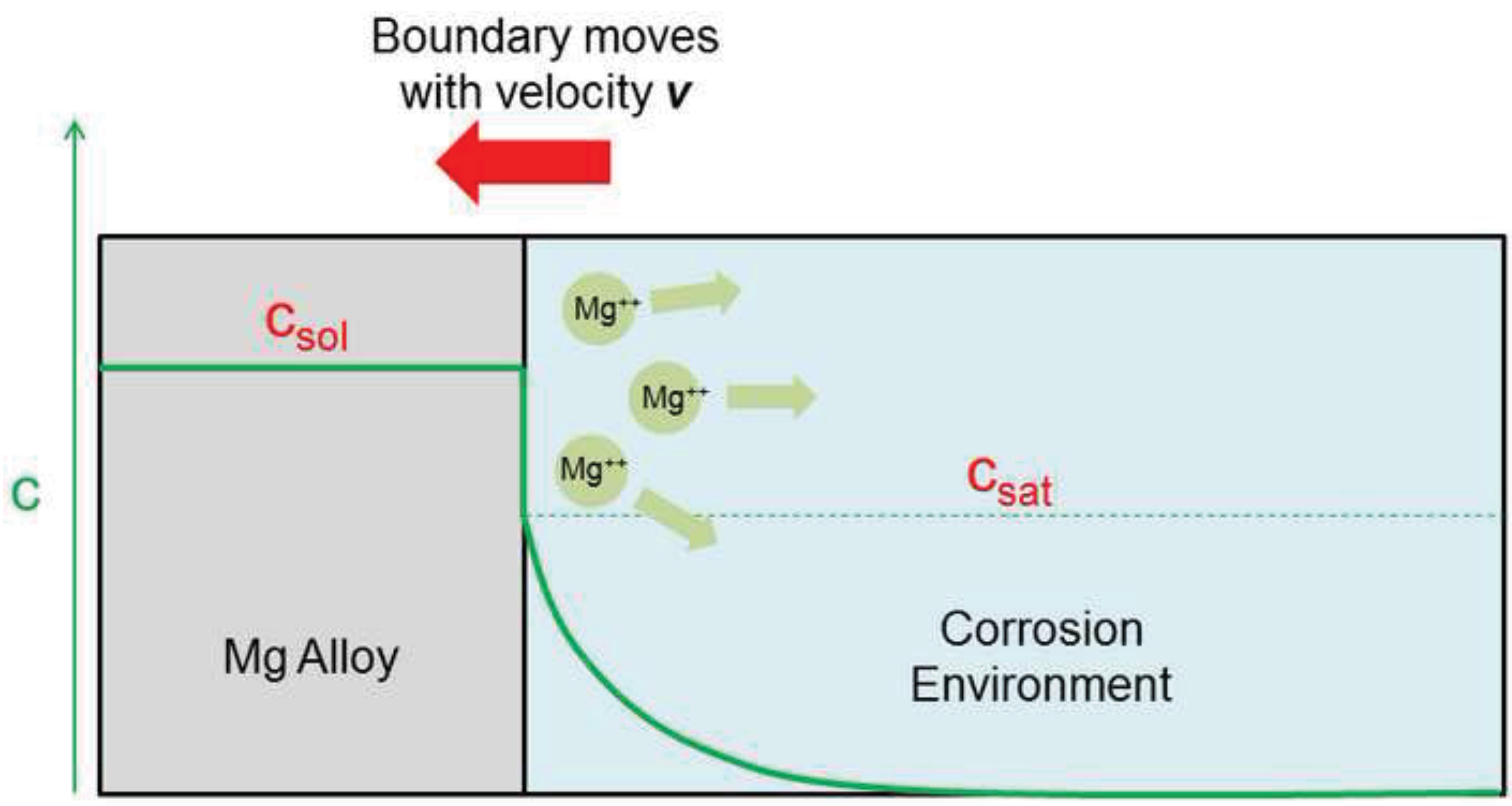
Boundary moves
with velocity v
C
C_{sol}
Mg Alloy
Mg++
Mg++
Mg++
C_{sat}
Corrosion
Environment

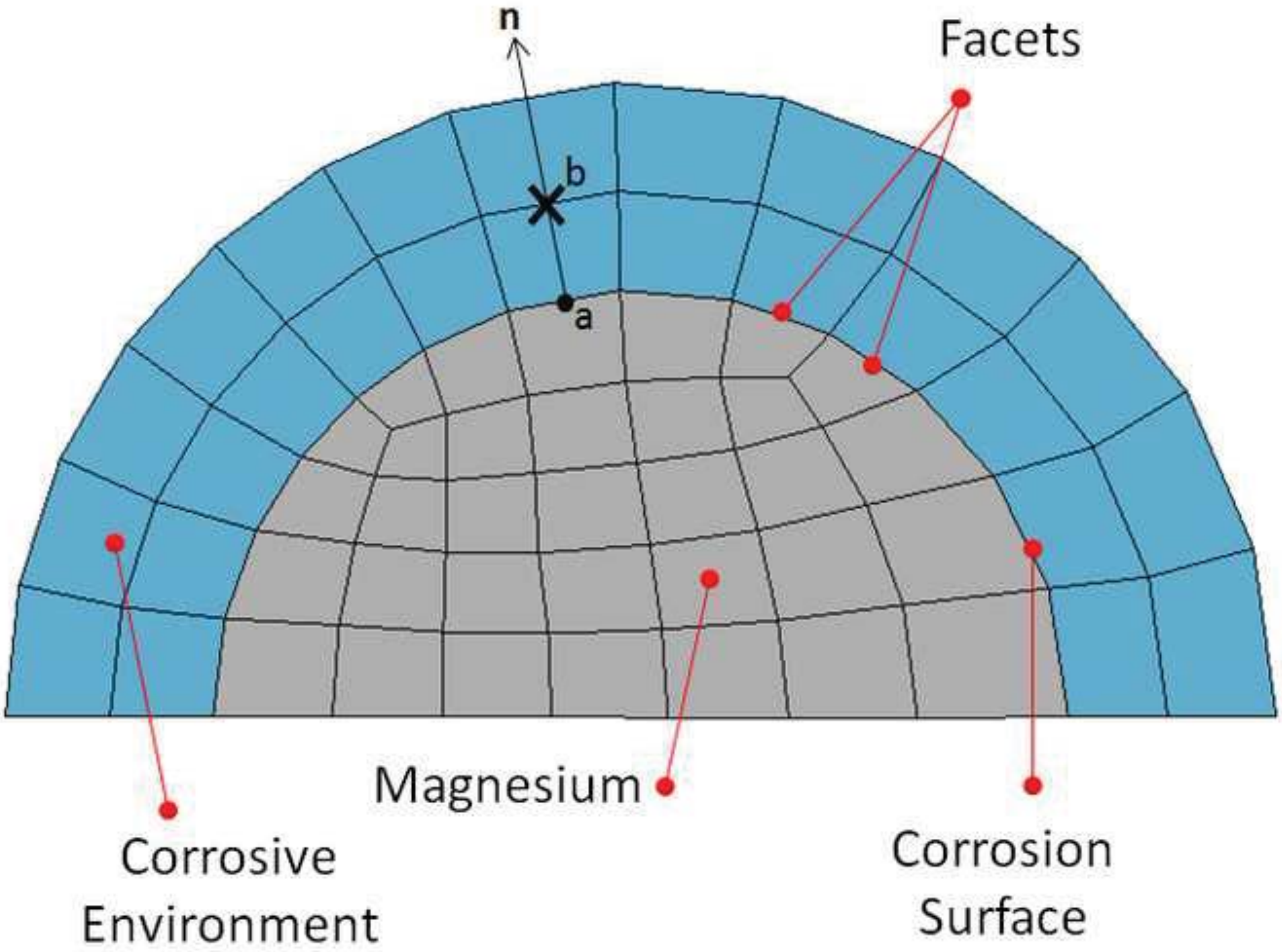
n
b
a
Facets
Magnesium
Corrosive
Environment
Corrosion
Surface

Fig3

Click here to download high resolution image

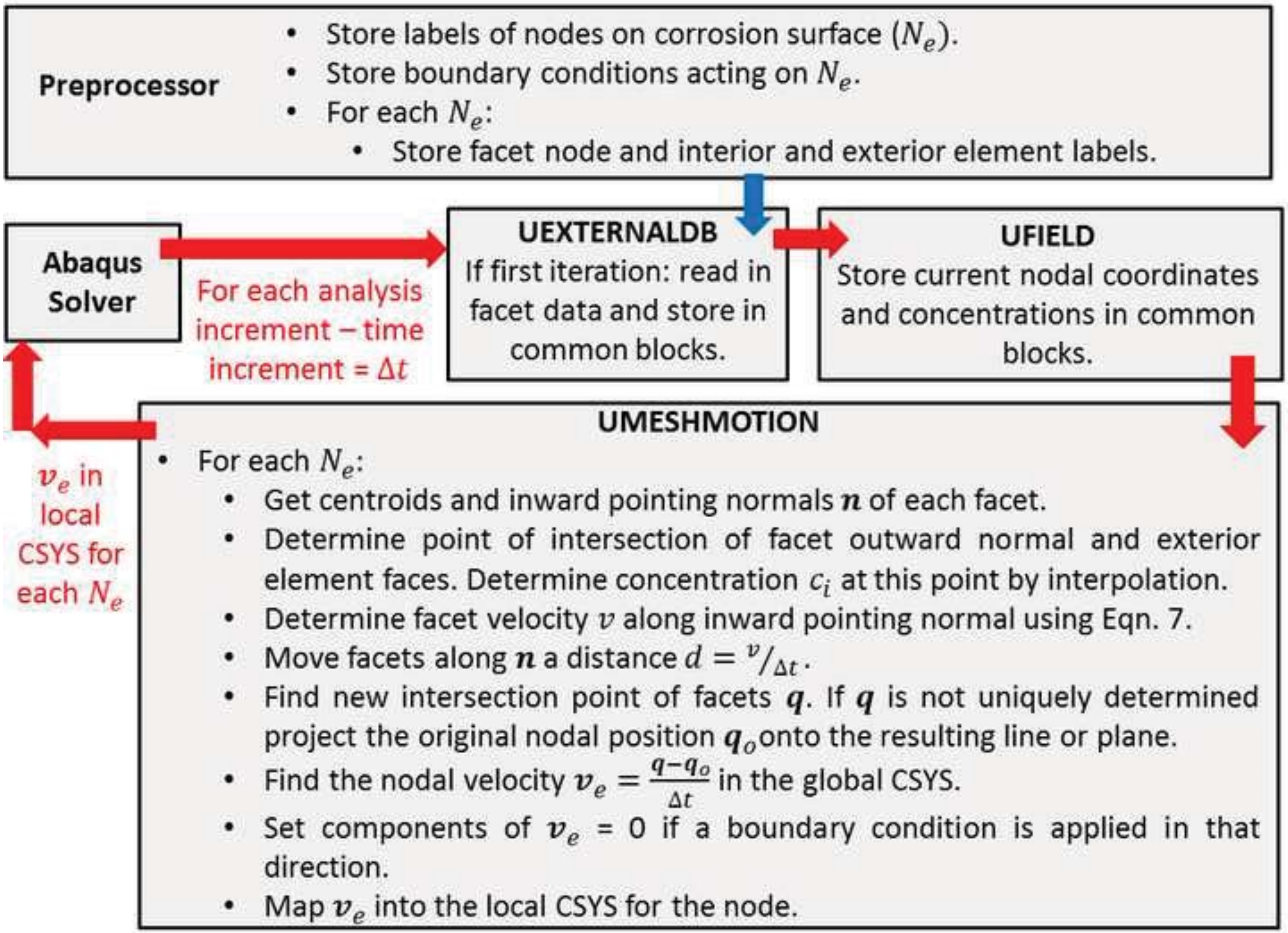

Fig4

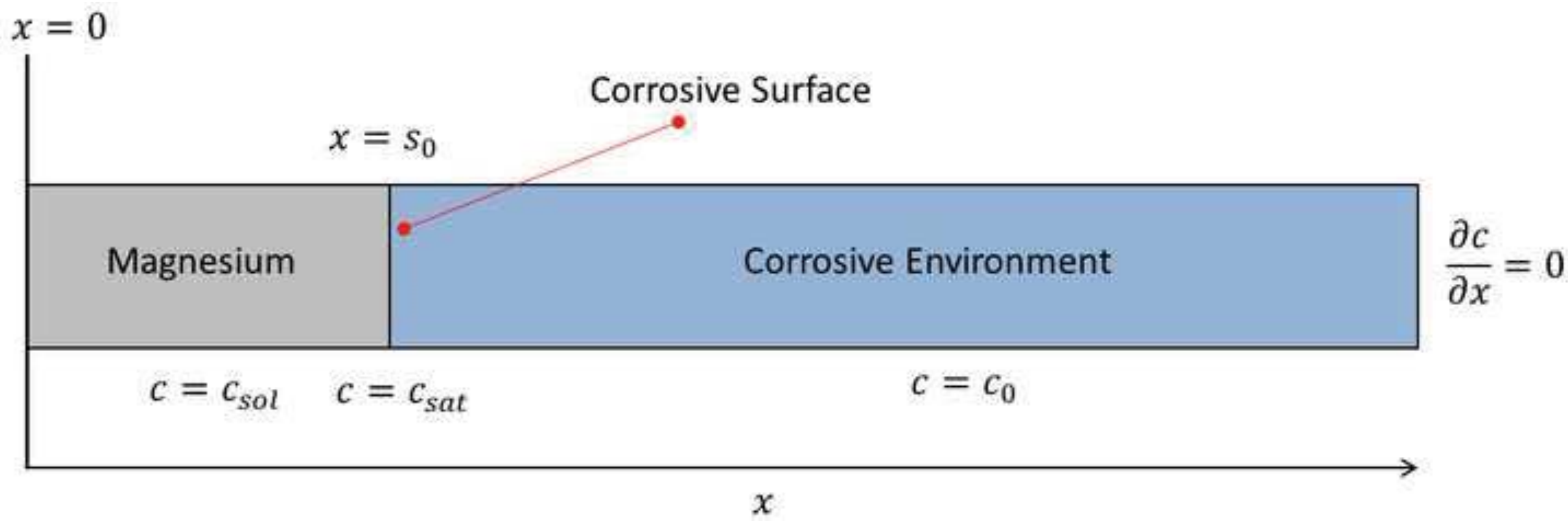

x = 0
Corrosive Surface
x = s0
Magnesium
Corrosive Environment
∂c/∂x = 0
c = csol
c = csat
c = c0
x

Fig5

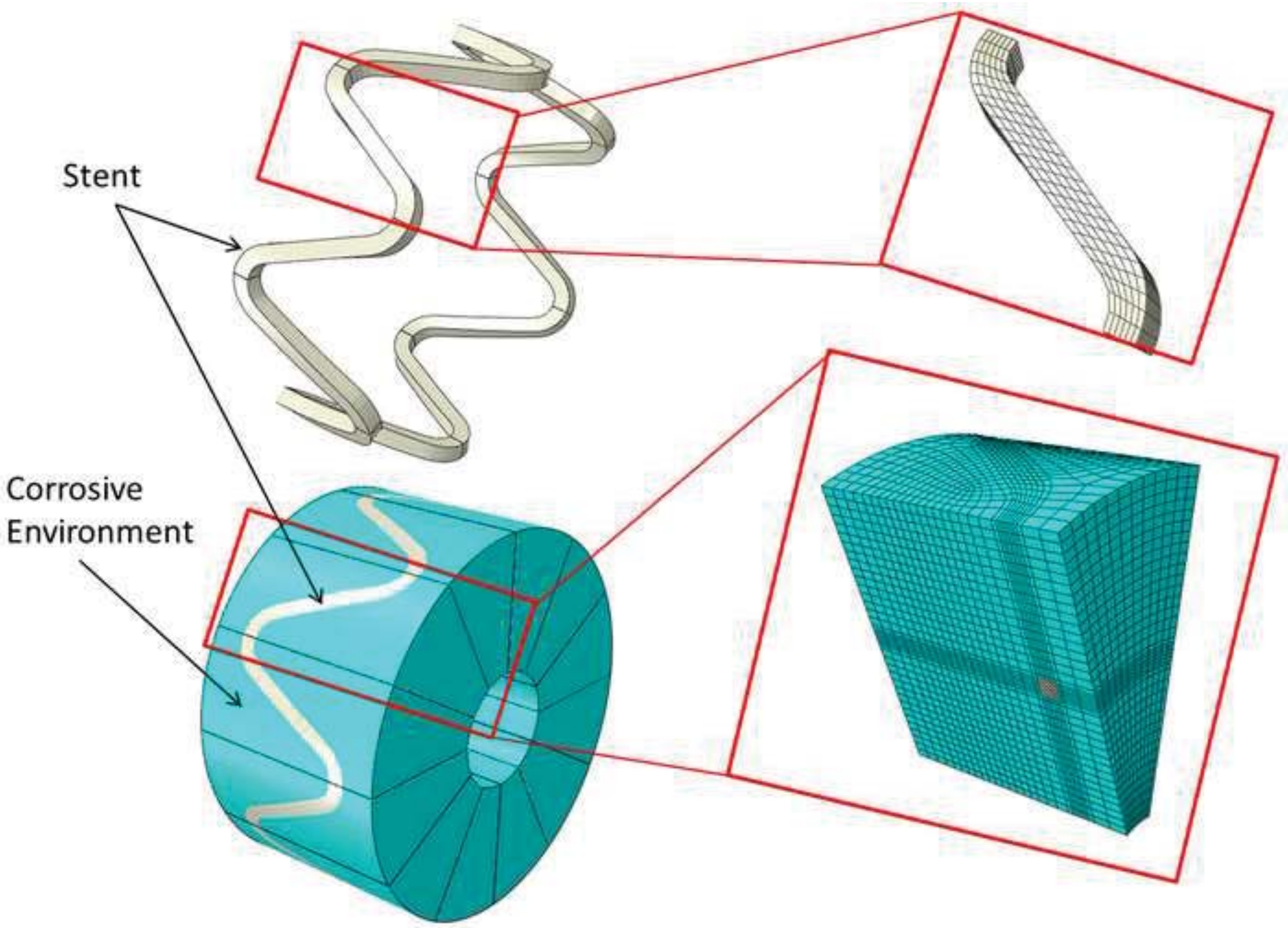

Fig6a

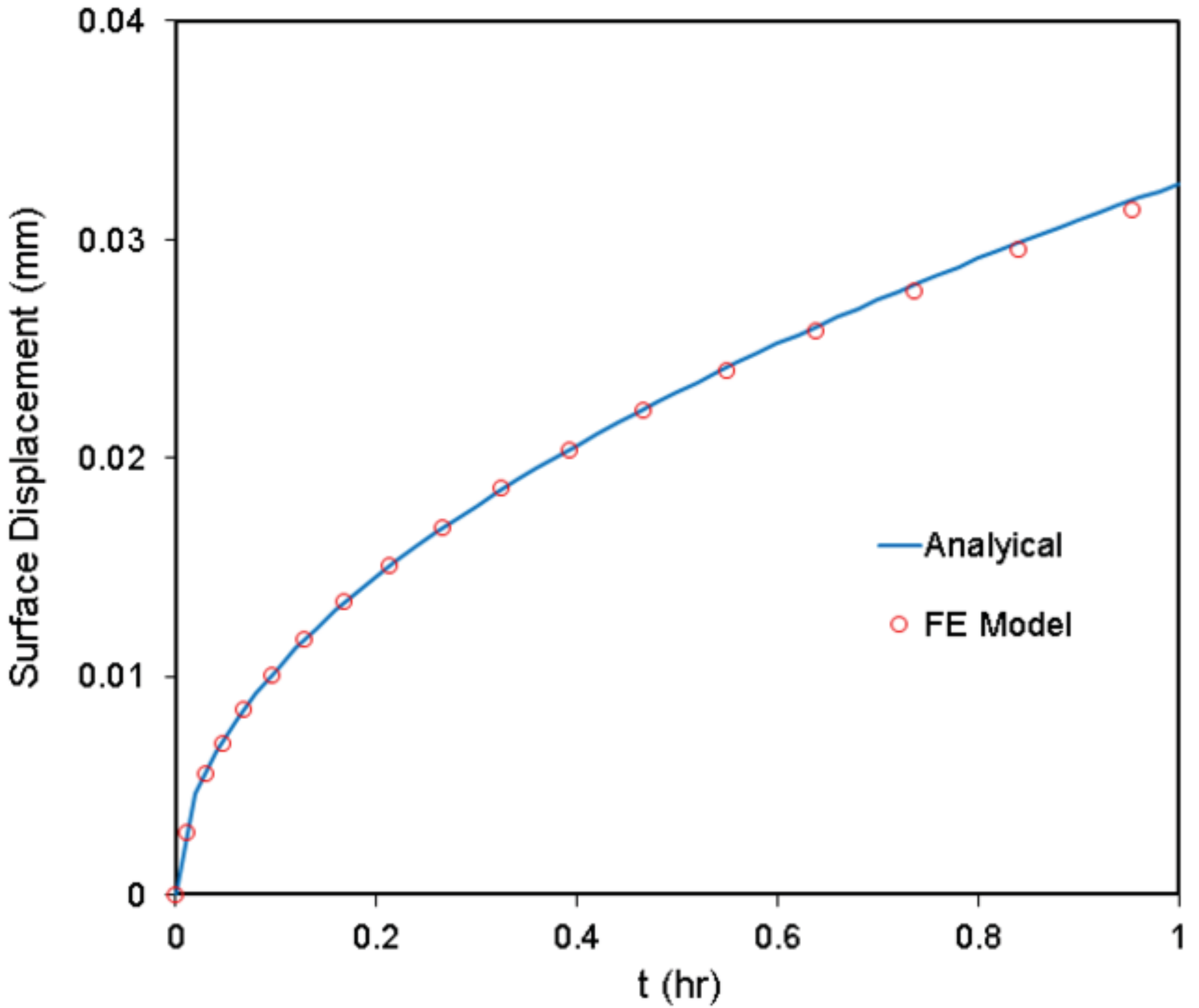
0.04
0.03
0.02
0.01
0
Surface Displacement (mm)
0
0.2
0.4
0.6
0.8
1
t (hr)
Analyical
FE Model

Fig6b

Click here to download high resolution image

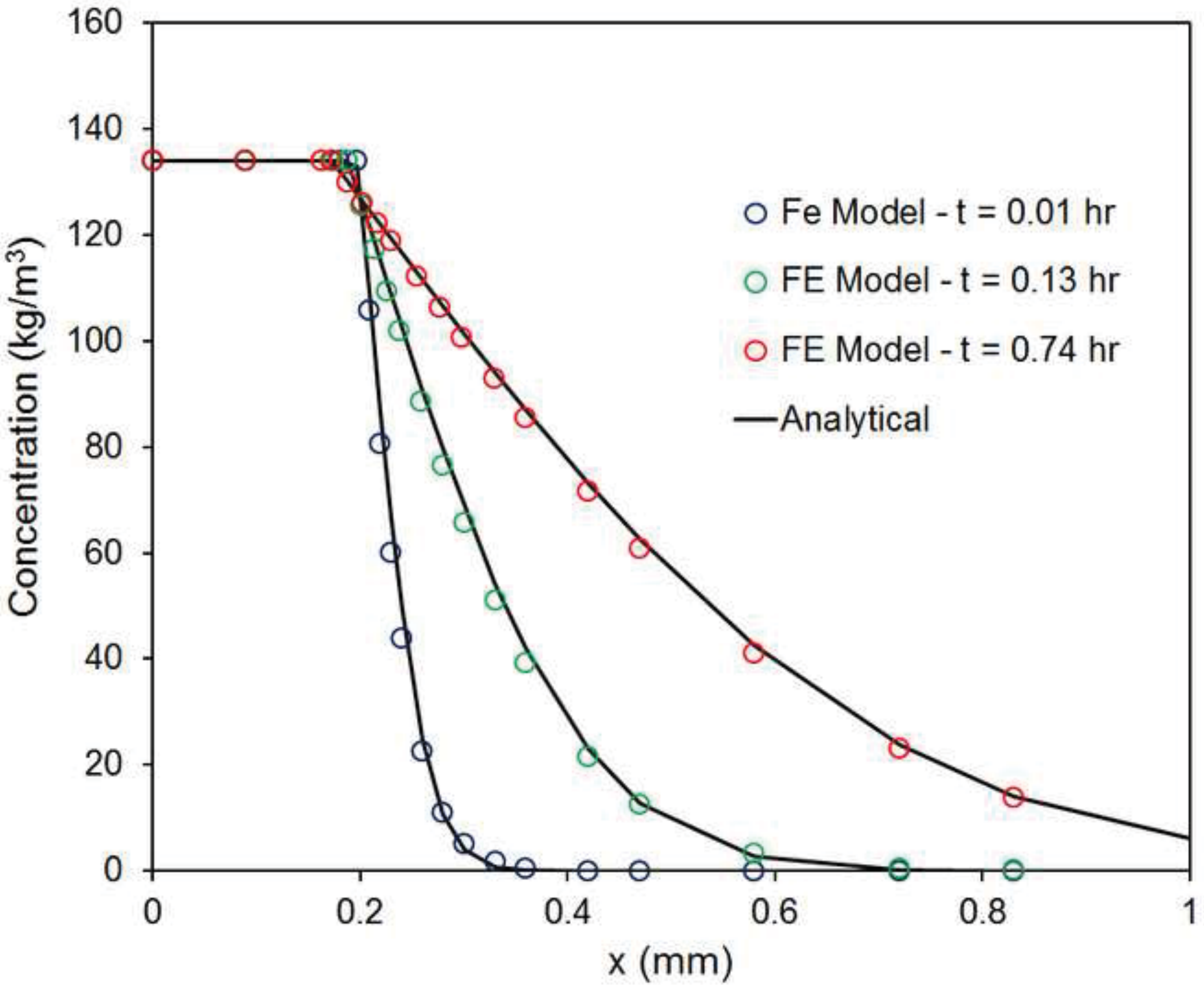

Fig7a

Click here to download high resolution image

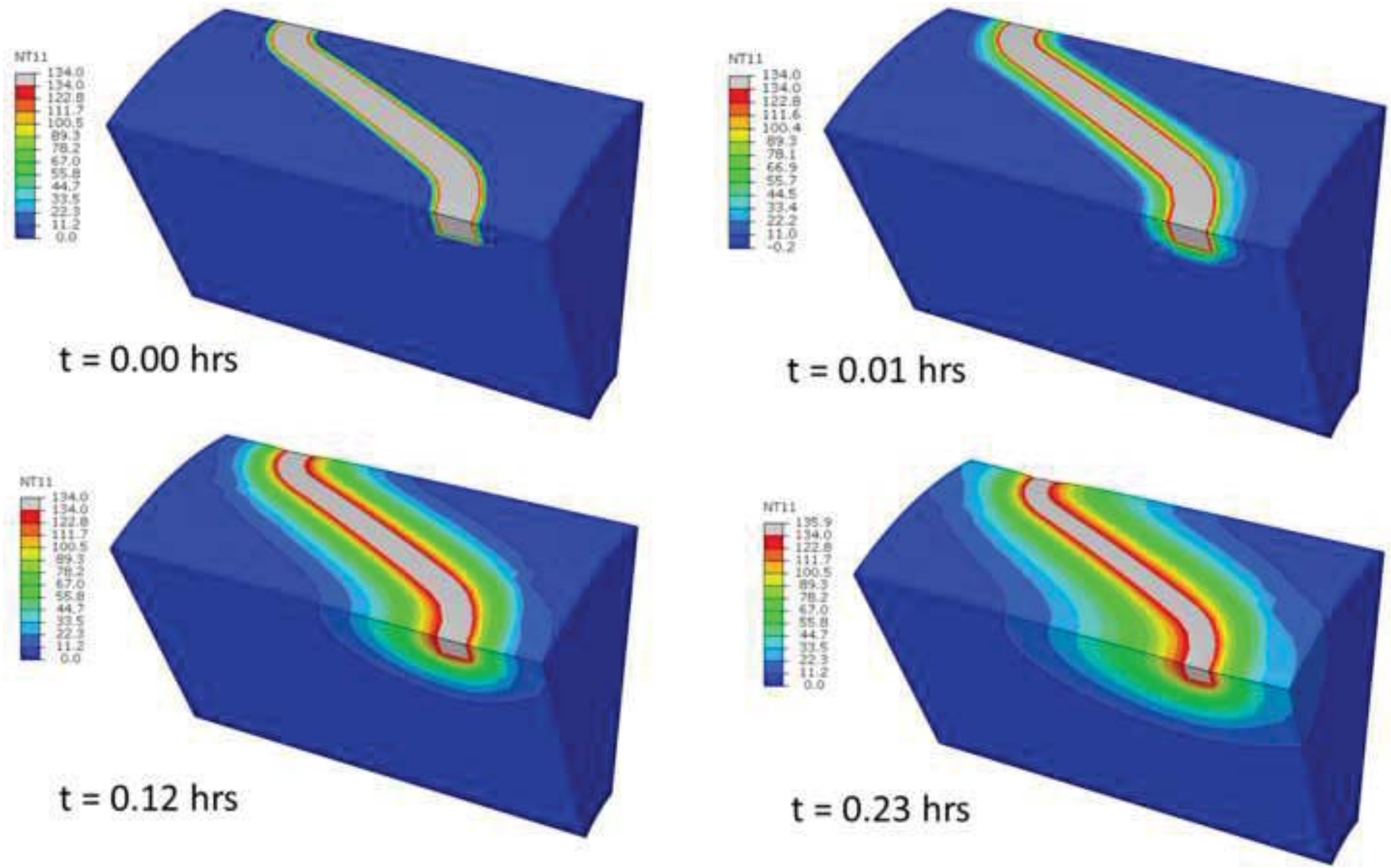

Fig7b

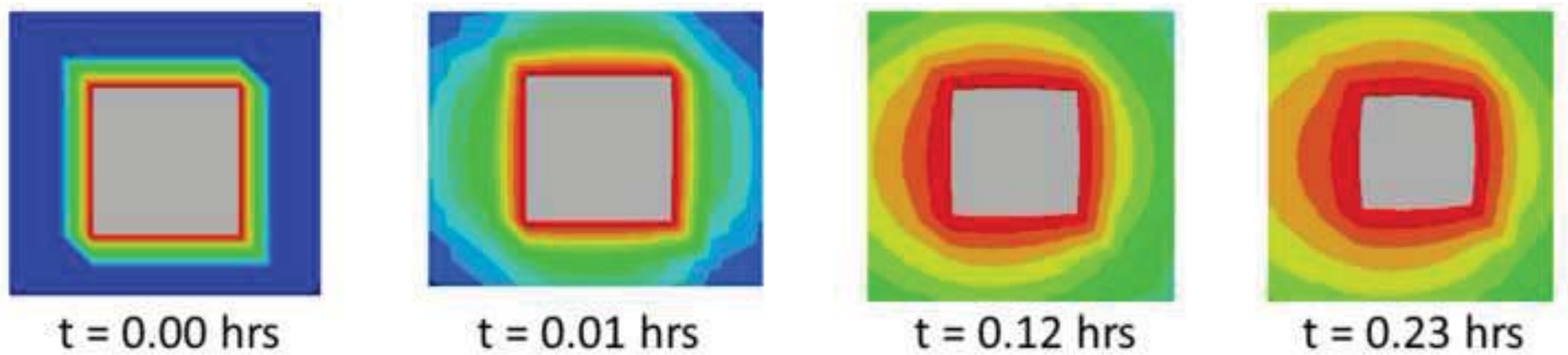

Fig8a

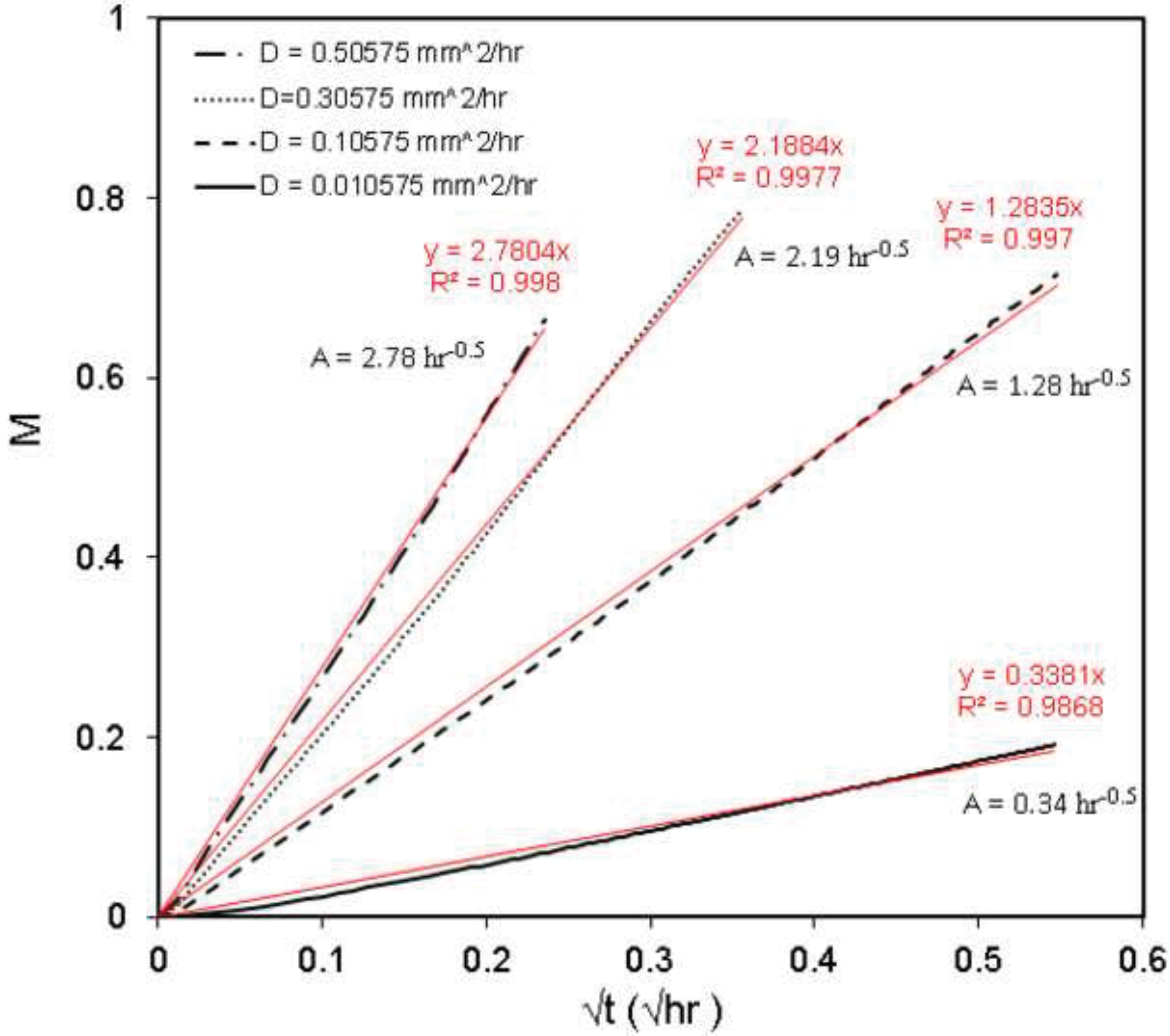
D = 0.50575 mm^2/hr
D=0.30575 mm^2/hr
D = 0.10575 mm^2/hr
D = 0.010575 mm^2/hr
y = 2.7804x
R² = 0.998
A = 2.78 hr-0.5
y = 2.1884x
R² = 0.9977
A = 2.19 hr-0.5
y = 1.2835x
R² = 0.997
A = 1.28 hr-0.5
y = 0.3381x
R² = 0.9868
A = 0.34 hr-0.5
M
√t (√hr)
0
0.2
0.4
0.6
0.8
1
0.1
0.3
0.5

Fig8b

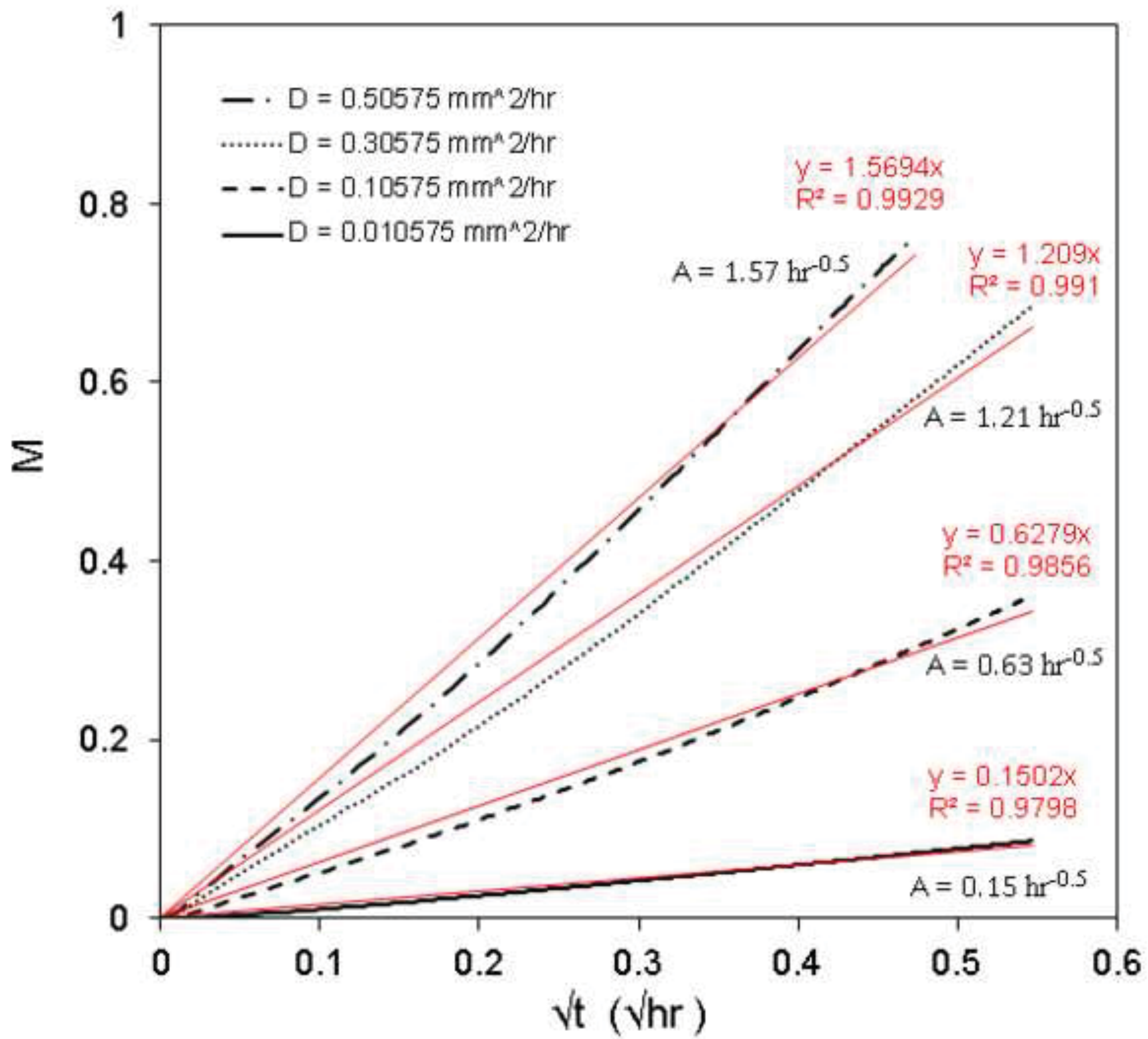
D = 0.50575 mm^2/hr
D = 0.30575 mm^2/hr
D = 0.10575 mm^2/hr
D = 0.010575 mm^2/hr
y = 1.5694x
R² = 0.9929
A = 1.57 hr-0.5
y = 1.209x
R² = 0.991
A = 1.21 hr-0.5
y = 0.6279x
R² = 0.9856
A = 0.63 hr-0.5
y = 0.1502x
R² = 0.9798
A = 0.15 hr-0.5
M
1
0.8
0.6
0.4
0.2
0
0.1
0.2
0.3
0.4
0.5
0.6
√t (√hr)

Fig9a

Click here to download high resolution image

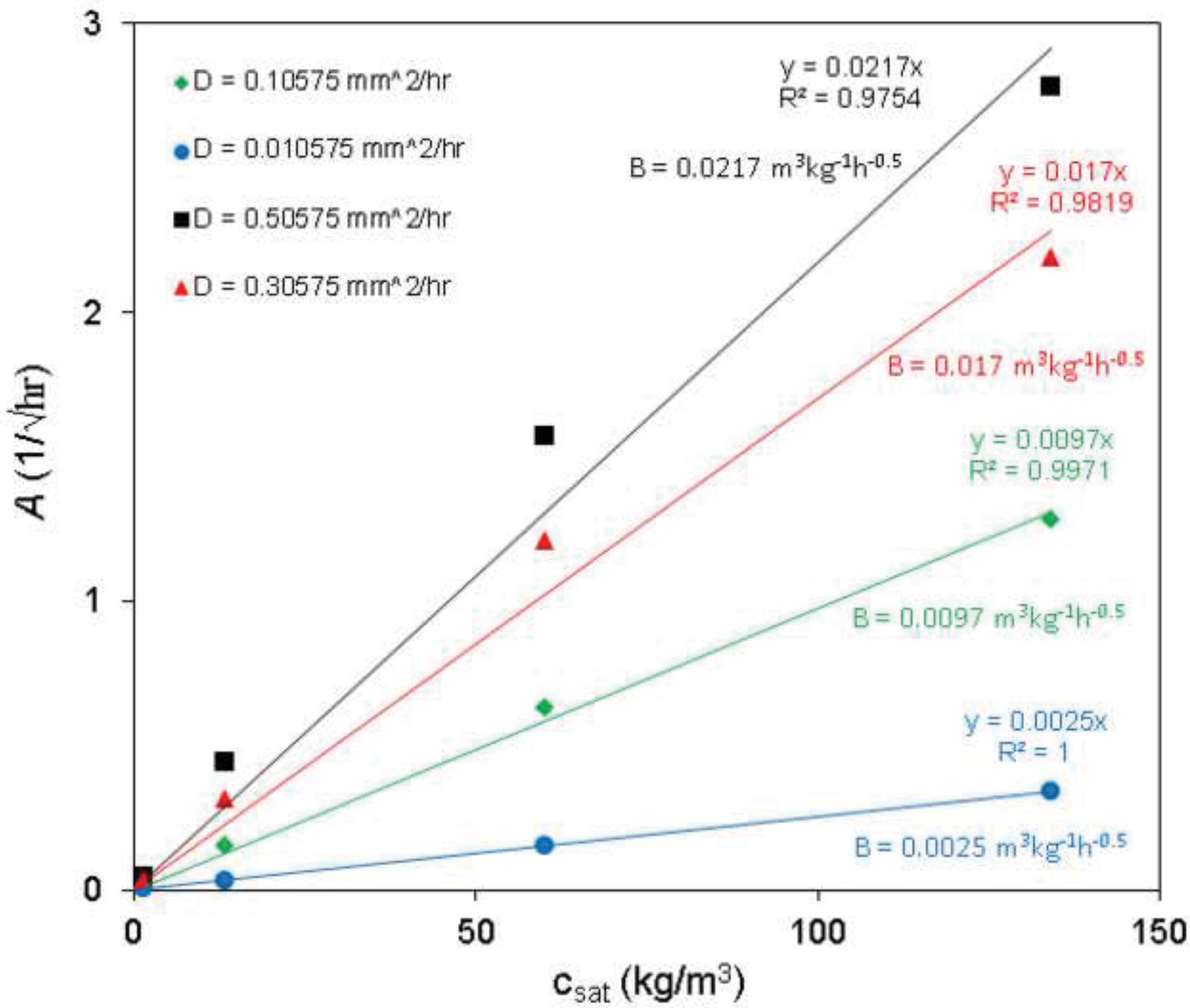

Fig9b

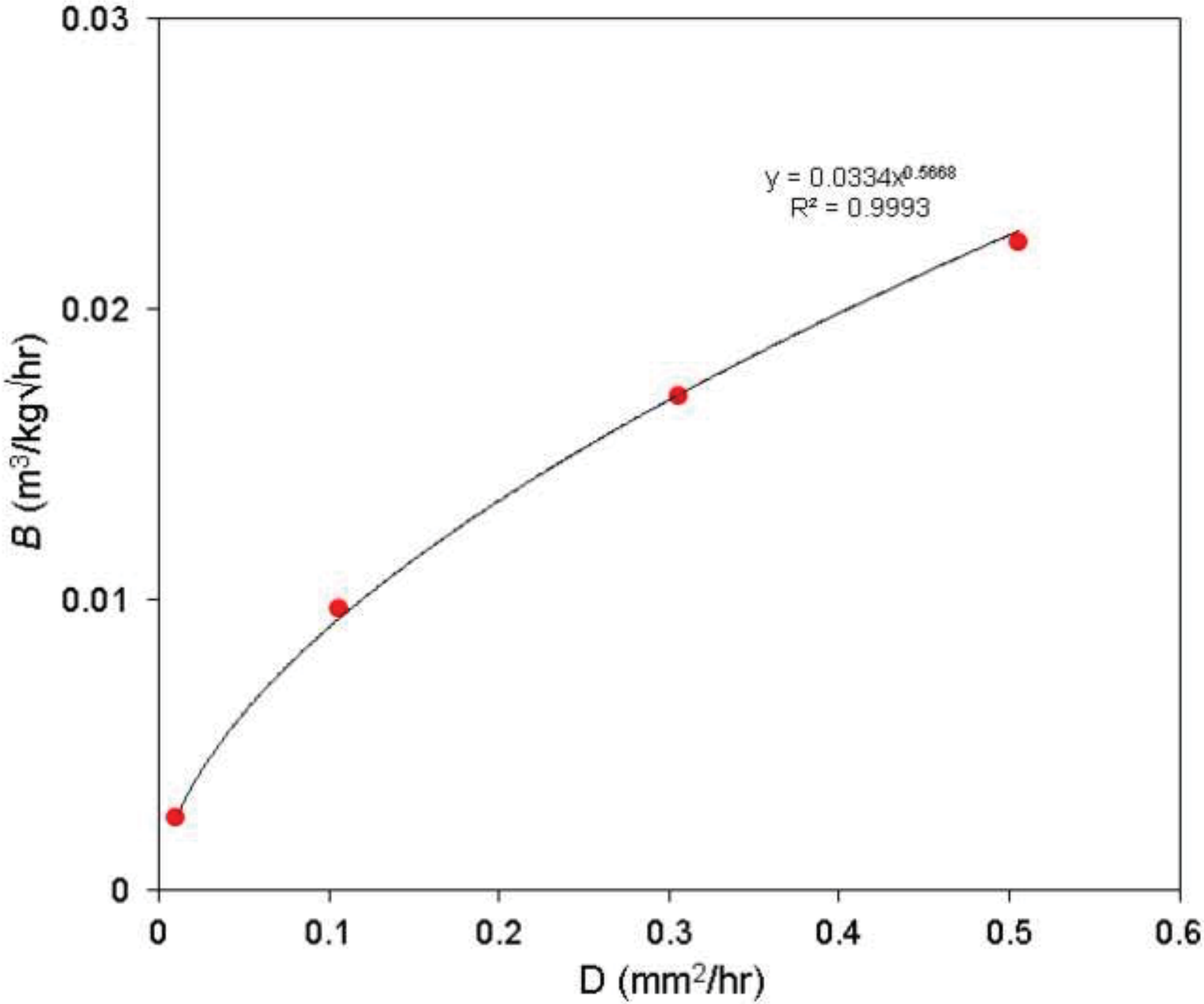
0.03
0.02
0.01
0
B (m³/kg√hr)
0
0.1
0.2
0.3
0.4
0.5
0.6
D (mm²/hr)
y = 0.0334x^0.5668
R² = 0.9993

Fig10a

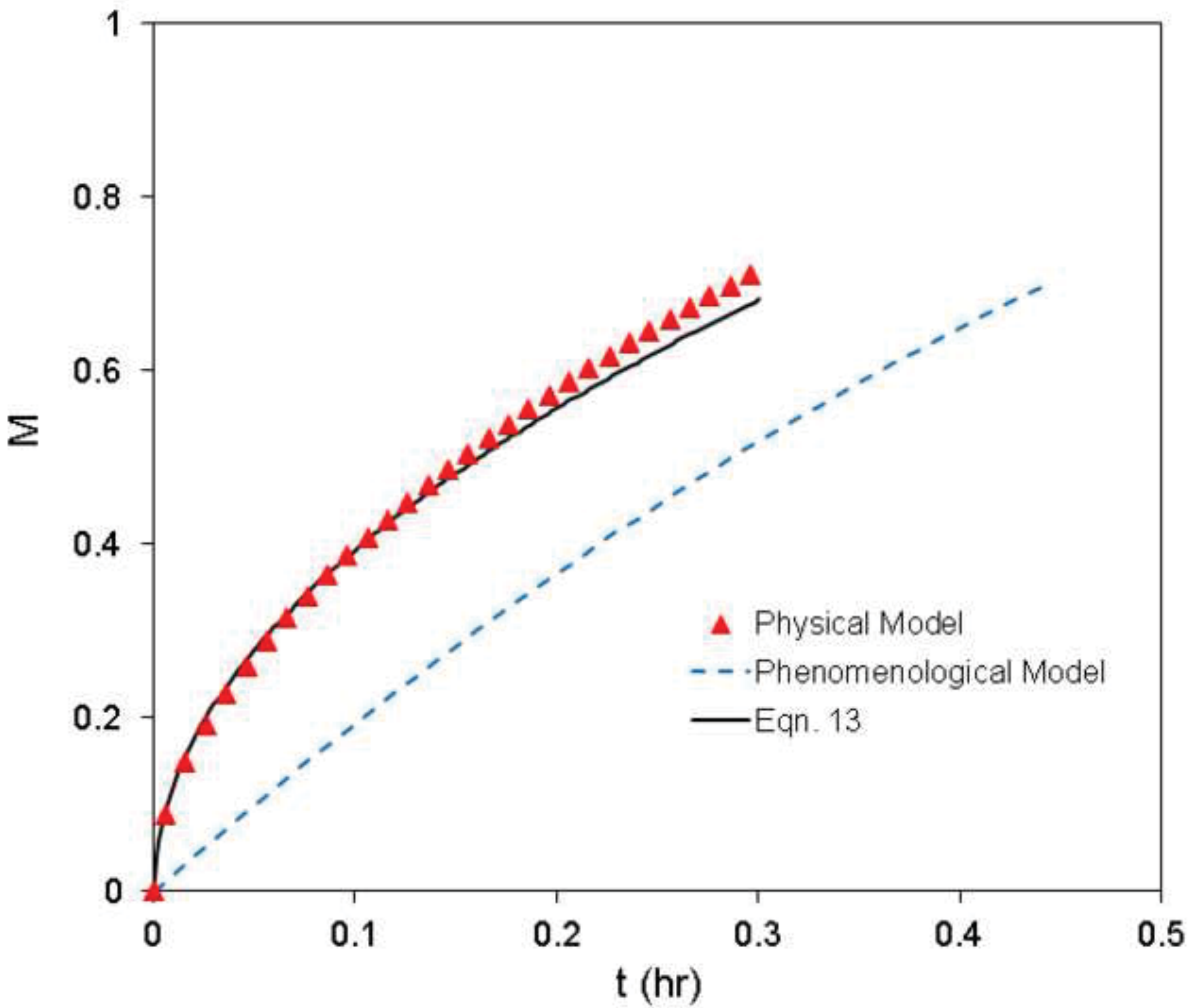
M
t (hr)
1
0.8
0.6
0.4
0.2
0
0
0.1
0.2
0.3
0.4
0.5
Physical Model
Phenomenological Model
Eqn. 13

Fig10b

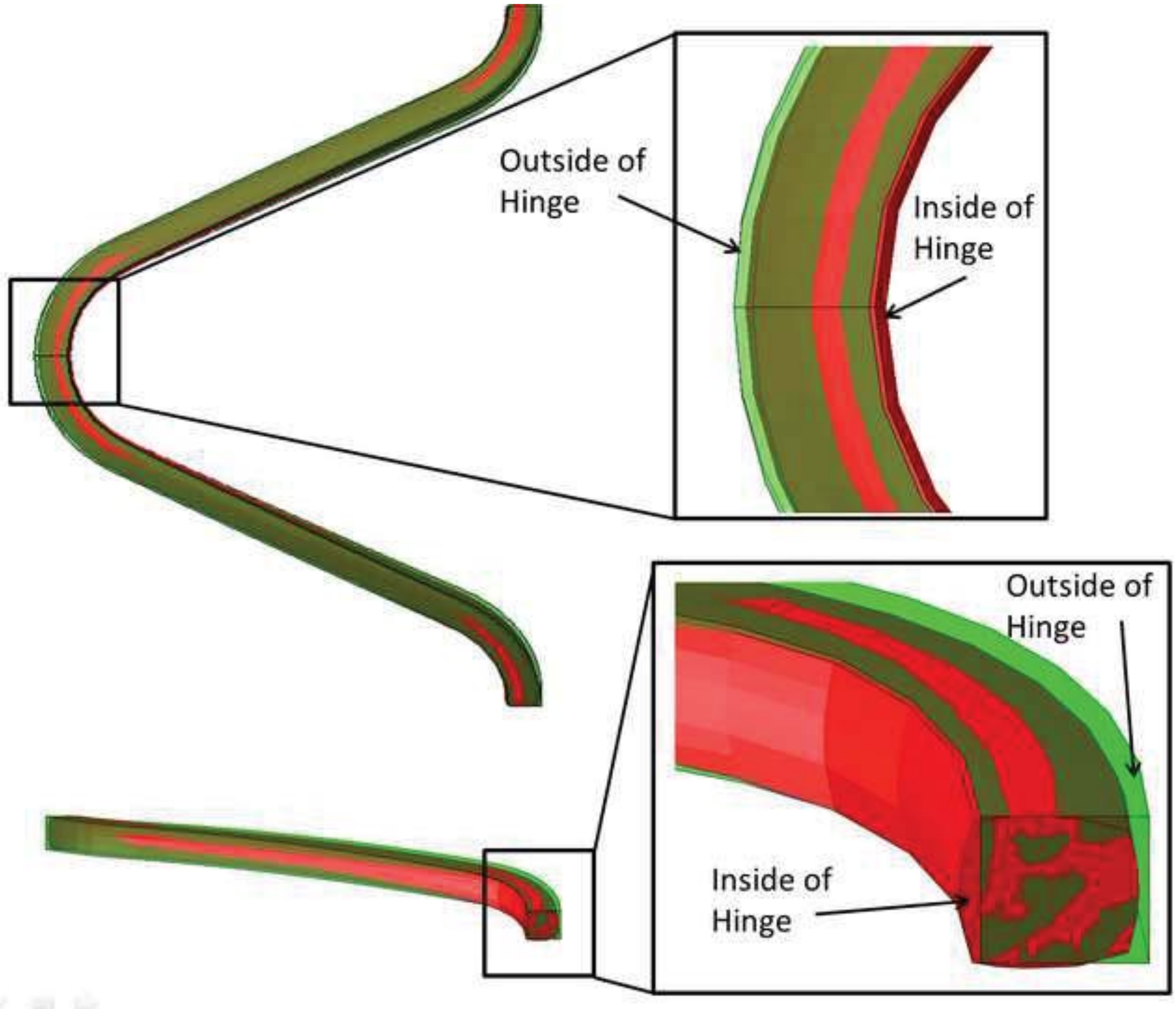
Outside of
Hinge
Inside of
Hinge
Outside of
Hinge
Inside of
Hinge

Fig11a
Click here to download high resolution image

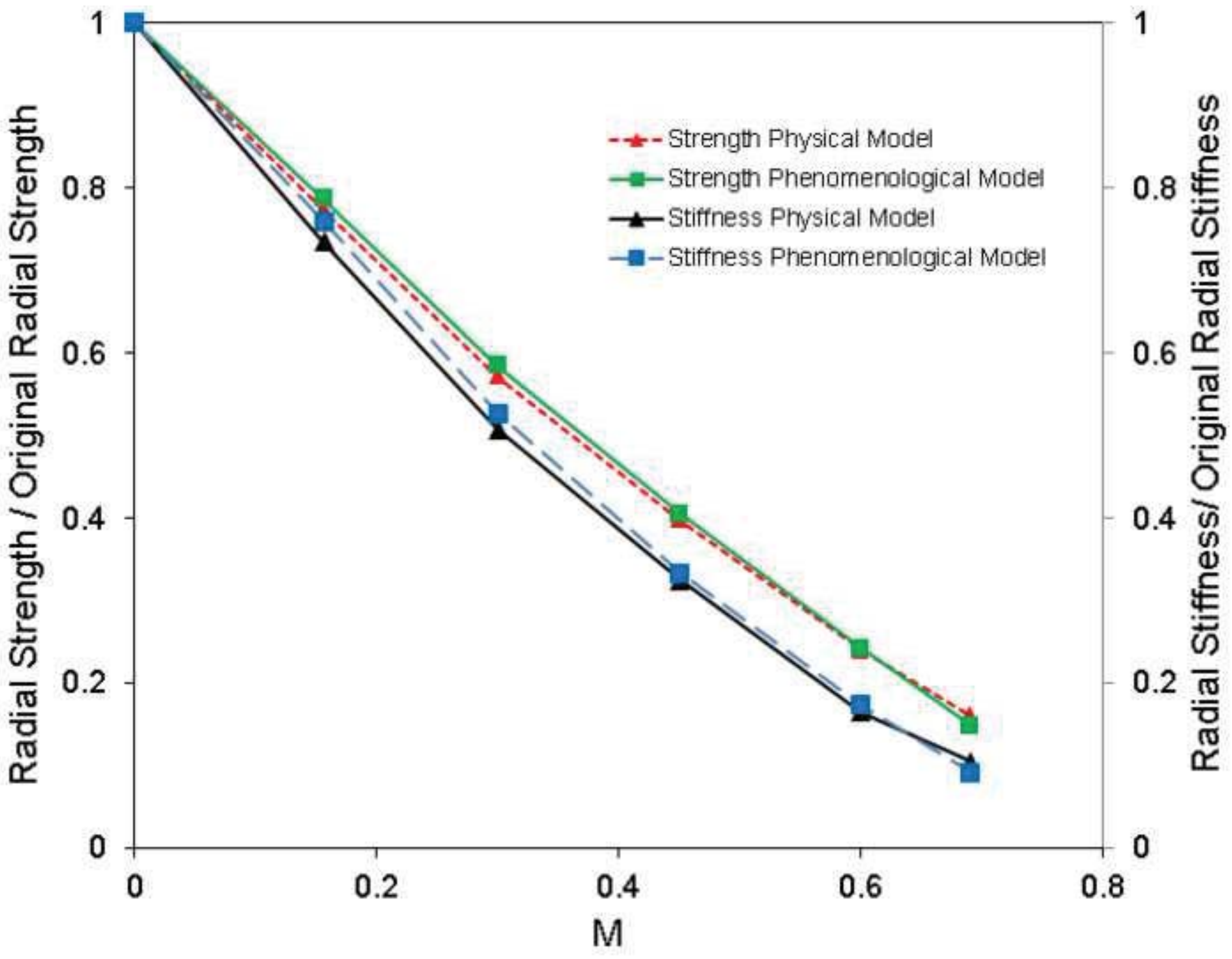

Fig11b

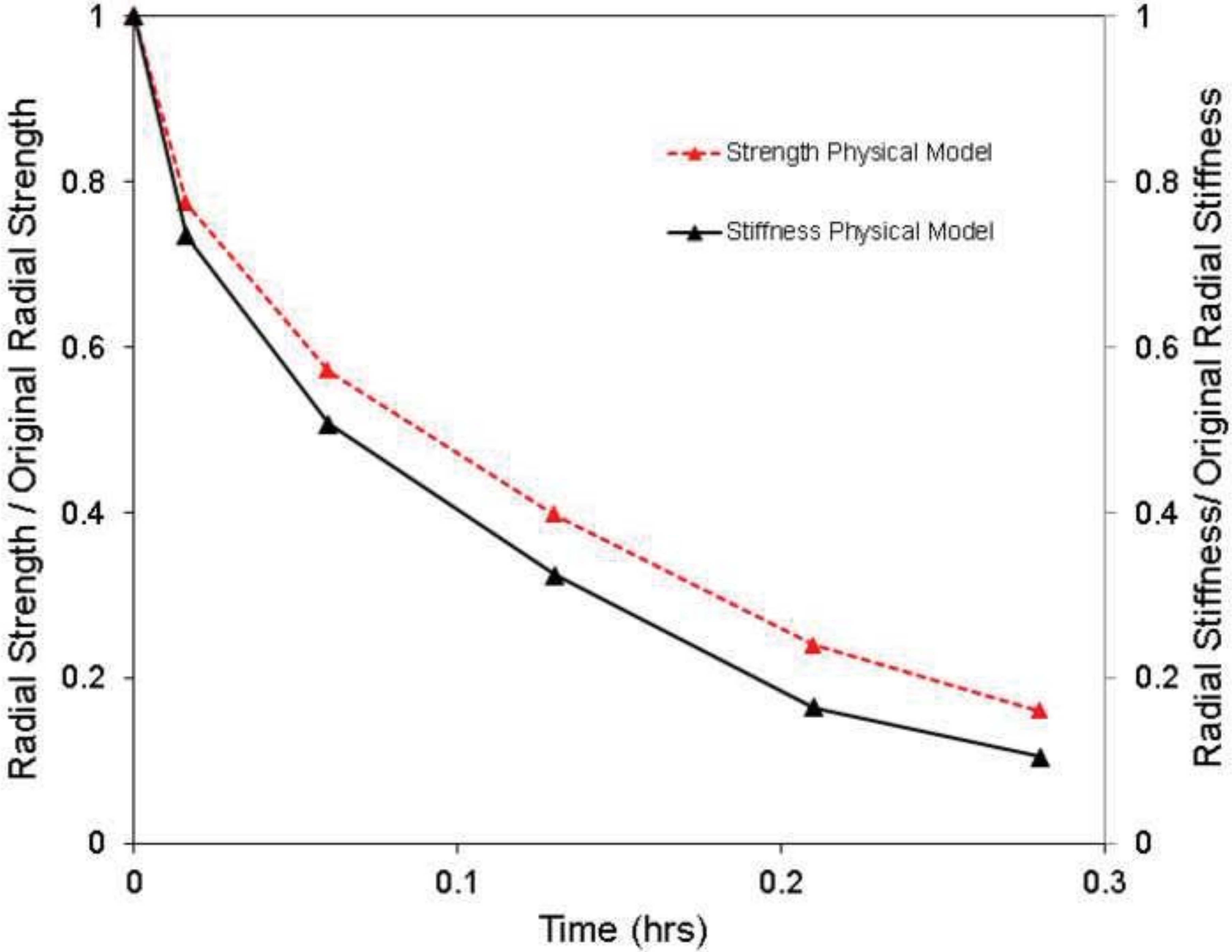
Strength Physical Model
Stiffness Physical Model
Radial Strength / Original Radial Strength
Radial Stiffness/ Original Radial Stiffness
Time (hrs)
0
0.1
0.2
0.3
0.2
0.4
0.6
0.8
1